The Emerald Research Register for this journal is available at
www.emeraldinsight.com/researchregister

The current issue and full text archive of this journal is available at
www.emeraldinsight.com/0961-5539.htm

Received March 2004
Revised October 2004
Accepted October 2004

Mixed convection with flow reversal in the entrance region of inclined tubes

Thierry Maré
Laboratoire de thermique des bâtiments, GRGC INSA de Rennes, Rennes, France
Nicolas Galanis
Faculté de génie, Université de Sherbrooke, Sherbrooke, QC, Canada, and
Sylvie Prétot and Jacques Miriel
Laboratoire de thermique des bâtiments, GRGC INSA de Rennes, Rennes, France

Abstract

Purpose – To determine the axial evolution of the hydrodynamic and the thermal fields for mixed convection in inclined tubes and to investigate the presence of flow reversal.

Design/methodology/approach – The elliptical, coupled, steady state, three-dimensional governing partial differential equations for heated ascending laminar mixed convection in an inclined isothermal tube were solved numerically using a finite volume staggered grid approach.

Findings – The axial evolution of the velocity profiles and fluid temperatures show that upstream diffusion has an important effect near the inlet of the heating region. As a result, both the wall shear stress and the Nusselt number are affected upstream of the heating zone. Flow reversal occurs of $GF \geq 9 \times 10^5$. The shape and size of the region with negative velocities depends strongly on the value of the Grashof number. The effect of the Grashof number on the axial evolution of the wall shear stress and the Nusselt number is shown to be very important in the region of developing flow.

Research limitations/implications – The results have been calculated for one Reynolds number (Re = 100), a single fluid (air) and one tube inclination (45°).

Practical implications – Further results of this type can be mapped and would be useful for heat exchanger design.

Originality/value – This is the first time that flow reversal has been calculated numerically for inclined tubes. Most previous studies concern horizontal or vertical tubes and use axially parabolic equations which are easier to solve but can not calculate the flow field in the region with backflow.

Keywords Flow, Diffusion, Numerical analysis, Convection

Paper type Research paper

Nomenclature

a	= thermal diffusivity ($m^2 s^{-1}$)	P	= pressure (Pa)
D	= tube diameter (m)	Pr	= Prandtl number
g	= acceleration of gravity ($m s^{-2}$)	R	= non-dimensional radial coordinate
Gr	= Grashof number	Re	= Reynolds number
L	= length of isothermal region (m)	T	= temperature (K)

International Journal of Numerical Methods for Heat & Fluid Flow
Vol. 15 No. 7, 2005
pp. 740-756

0961-5539
DOI 10.1108/09615530510613906

V = velocity ($m\,s^{-1}$)
x, y = cartesian coordinates (m)
Z = axial coordinate (m)

Greek letters

α = tube inclination
β = thermal expansion coefficient (K^{-1})
μ = viscosity ($N\,s\,m^{-2}$)
ρ = density ($kg\,m^{-3}$)
τ = non-dimensional shear stress
ϕ = circumferential coordinate

Indices

o = inlet conditions
R, Z = radial, axial component
w = wall value
ϕ = circumferential component

1. Introduction

Combined forced and free convection in the entrance region of tubes occurs in many engineering installations such as heat exchangers, nuclear reactors, solar collectors, etc. The secondary flow induced by the buoyancy force and its effects on the hydrodynamic and thermal fields have therefore been investigated both experimentally and numerically. Piva *et al.* (2000) have recently compiled an extensive list of articles dealing with this problem. Most such studies deal with flow in horizontal or vertical tubes even though inclined tubes are often used in practice. The few numerical studies which have considered mixed convection in inclined tubes (Choudhury and Patankar, 1988; Orfi *et al.*, 1998; Ouzzane and Galanis, 1999) have used the three-dimensional axially parabolic formulation proposed by Patankar and Spalding (1972). By neglecting the axial diffusion of heat and momentum, this approach permits a marching integration calculation procedure. It thus reduces the computer memory needed to solve the partial differential equations modelling the flow field but cannot predict either the effects of upstream diffusion of momentum and heat or those of flow reversal.

During the last three decades, some attention has been paid to the effects of axial diffusion of momentum and heat, mostly for pure forced convection. Thus, the distinct analyses of hydrodynamic and thermal laminar entrance problems (Shah and London, 1978) provide the limits beyond which axial diffusive transport can be neglected: momentum axial diffusion can be neglected far from the immediate entrance provided $Re > 400$ while axial diffusion of heat can be neglected for $Pe > 10$ when the wall heat flux is uniform, and for $Pe > 50$ when the wall temperature is uniform. Pagliarini (1989) investigated these effects for simultaneously developing forced convection and concluded that the criterion for the inclusion of the axial diffusion terms should be based on both the Reynolds and Péclet (or Prandtl) numbers. Nesreddine *et al.* (1998) in their numerical study of laminar mixed convection of air, with aiding or opposing buoyancy, mapped the conditions that give rise to significant preheating and flow reversal on a Grashof-Reynolds plane. They thus established criteria that determine

(1) when the inlet boundary conditions can be applied at the beginning of the heated section of the tube, and
(2) when the elliptical formulation is necessary to describe the flow field accurately.

Flow reversal in vertical tubes has been observed experimentally (Bernier and Baliga, 1992) and predicted numerically (Nesreddine *et al.*, 1995; Zghal *et al.*, 2001). The study by Zghal *et al.* (2001), who used a 2D elliptical formulation to model the developing laminar flow field for ascending air flow in a uniformly-heated vertical tube, presents an interesting chart, which defines the critical combinations of Re, Gr and heating

length leading to flow reversal. Wang *et al.* (1994) have analysed mixed convection with flow reversal in both vertical and horizontal tubes using a 3D elliptical model for the laminar flow field. All of these studies show that flow reversal has important effects on the Nusselt number and on the friction factor.

In view of the demonstrated important effects of axial diffusion and flow reversal on mixed convection, and the lack of relevant information for such conditions in inclined tubes, the present research program has been undertaken. It includes the numerical prediction and the experimental visualisation of such flow fields. In this paper we present the numerically predicted effect of the Grashof number on the axial velocity distribution for ascending heated air flow in an inclined isothermal tube. Particular emphasis is placed on the shape and size of the region with negative axial velocities (i.e. velocities opposite to the direction of the mass flow) and on the effect of these negative velocities on the friction coefficient and on the Nusselt number. The sofware used in this study can eventually be adapted for the design of heat exchangers and the prdiction of their off-design performance.

2. Mathematical formulation and numerical scheme

The problem under consideration and the coordinate system are shown in Figure 1. A Newtonian fluid enters the inclined tube at $Z = -10D$ with uniform temperature T_o and velocity V_o. The solid-fluid interface is adiabatic between $Z = -10D$ and $Z = 0$ while the rest of the interface from $Z = 0$ to $Z = L$ is isothermal ($T_w > T_o$). The following assumptions are introduced:

- The fluid properties are constant except for the density whose variation is considered only in the buoyancy terms and modelled using the Boussinesq approximation:

$$\rho = \rho_o[1 - \beta(T - T_o)] \tag{1}$$

- The flow is laminar, steady and three-dimensional.
- Viscous dissipation is neglected as in all the numerical studies cited in the introduction.

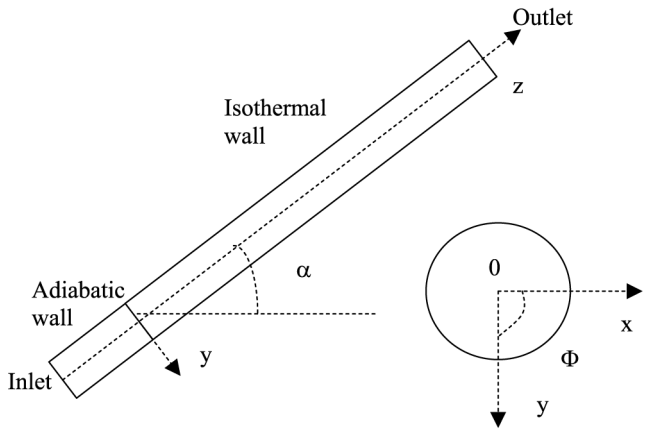

Figure 1.
Schematic representation of system under study

With these assumptions, the governing equations in cylindrical coordinates are as follows:

$$\frac{1}{R}\frac{\partial}{\partial R}(RV_R) + \frac{1}{R}\frac{\partial V_\phi}{\partial \phi} + \frac{\partial V_Z}{\partial Z} = 0 \tag{2}$$

$$\rho\left(V_R\frac{\partial V_R}{\partial R} + \frac{V_\phi}{R}\frac{\partial V_R}{\partial \phi} - \frac{V_\phi^2}{R} + V_Z\frac{\partial V_R}{\partial Z}\right) = \mu\left(\nabla^2 V_R - \frac{V_R}{R^2} - \frac{2}{R^2}\frac{\partial V_\phi}{\partial \phi}\right) - \frac{\partial P}{\partial R} - \rho\ g\ \cos\alpha\ \cos\phi \tag{3}$$

$$\rho\left(V_R\frac{\partial V_\phi}{\partial R} + \frac{V_\phi}{R}\frac{\partial V_\phi}{\partial \phi} + \frac{V_\phi V_R}{R} + V_Z\frac{\partial V_\phi}{\partial Z}\right) = \mu\left(\nabla^2 V_\phi - \frac{V_\phi}{R^2} - \frac{2}{R^2}\frac{\partial V_R}{\partial \phi}\right) - \frac{1}{R}\frac{\partial P}{\partial \phi} + \rho\ g\ \cos\alpha\ \sin\phi \tag{4}$$

$$\rho\left(V_R\frac{\partial V_Z}{\partial R} + \frac{V_\phi}{R}\frac{\partial V_Z}{\partial \phi} + V_Z\frac{\partial V_Z}{\partial Z}\right) = \mu\nabla^2 V_Z - \frac{\partial P}{\partial Z} - \rho\ g\ \sin\alpha \tag{5}$$

$$V_R\frac{\partial T}{\partial R} + \frac{V_\phi}{R}\frac{\partial T}{\partial \phi} + V_Z\frac{\partial T}{\partial Z} = a\nabla^2 T \tag{6}$$

This system of coupled, non-linear partial differential equations is subject to the inlet (at $Z = -10D$) and interface (at $R = 0.5$) conditions described above. Since the formulation is elliptical, boundary conditions must also be specified at the tube outlet ($Z = L$). At that position, outflow conditions (Fluent 6.1 User's Guid, n.d.) are specified.

The system of PDEs is discretized with the control volume technique. A first order upwind method is used to interpolate the variables while the PISO algorithm is introduced for the velocity-pressure coupling. The pressure is calculated with a body-force weighed scheme and a segregated solution method is used to solve the discrete equations sequentially (Fluent 6.1 User's Guid, n.d.). The discretisation grid is uniform in the circumferential direction and non-uniform in the other two directions. It is finer near the heated tube inlet ($Z = 0$) and near the wall ($R = 0.5$) where the velocity and temperature gradients are large. Three different grid distributions ($250 \times 36 \times 31$, $200 \times 40 \times 31$ and $300 \times 40 \times 31$ in the axial, circumferential and radial directions respectively) have been tested in the heating region ($0 \leq Z \leq L$). Comparisons of velocity and temperature profiles at different axial positions have shown that the results predicted by the two grids with the higher number of axial grids are essentially identical (Voicu, 2002). In view of these results the adopted grid has 312480 nodes ($250 \times 36 \times 31$ in the heating region plus $30 \times 36 \times 31$ in the adiabatic entry zone). Figure 2 shows a comparison of velocity and temperature profiles calculated with the selected grid and corresponding experimental results by Zeldin and Schmidt (1972). The agreement is very good except for the temperature very close to the tube inlet where, according to the authors of the experimental study, axial conduction in the tube walls distorts the measured temperature profiles. The numerical results obtained in the

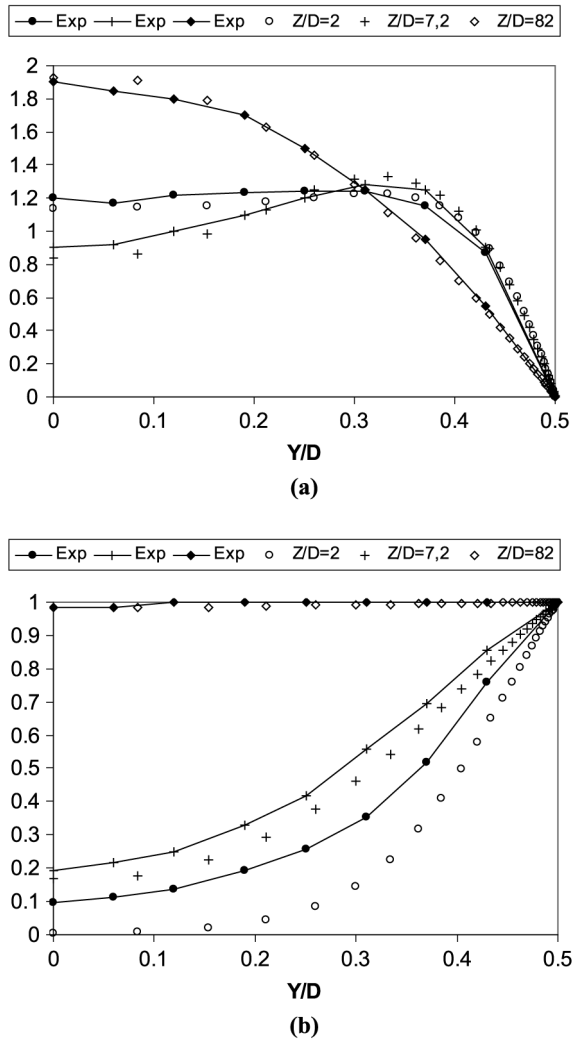

Figure 2.
Comparison of numerical results with measurements by Zeldin and Schmidt (1972) in (a) non-dimensional axial velocity, (b) non-dimensional temperature

present study are very close to those calculated by Zeldin and Schmidt (1972) as well as Collins (1980) who pointed out the importance of using an elliptical formulation such as the one used here. In view of these results we consider that the model, the numerical code and the selected grid are valid and can be used for the purposes of the present study.

3. Results and discussion

The results are presented in non-dimensional form. Reference quantities are the tube diameter D, the mean axial velocity V_o and the temperature difference $(T_w - T_o)$. With this formulation, the solution depends on the values of four parameters: the tube

inclination as well as the Prandtl, Reynolds and Grashof numbers (or, equivalently, the Prandtl, Péclet and Richardson numbers). All the results presented here were calculated with $\alpha = 45°$, $Pr = 0.7$, $Re = 100$ and $L/D = 106.7$ for different Grashof numbers (i.e. different wall temperatures and a constant $T_o = 295.75\,K$) up to $Gr = 1.5 \times 10^6$.

Figures 3a-d show the axial evolution of the non-dimensional fluid temperature near the wall ($R = 0.45$) at three different circumferential positions ($\phi = \pi/2$ and $\phi = -\pi/2$ correspond respectively to the top and bottom of the tube) for four different increasing values of the Grashof number. They also show the corresponding evolution of the non-dimensional average fluid temperature. It is noted that the latter, which is equal to zero in the adiabatic entry region, starts changing very soon after the beginning of the heated region. This distance which is approximately equal to D for $Gr = 1.5 \times 10^5$ decreases as the Grashof number (or, equivalently, the wall temperature) increases. Furthermore, the average fluid temperature approaches the wall temperature (the corresponding non-dimensional value tends to 1) at a distance from the beginning of the heated region which also decreases as Gr increases. These results indicate that the thermal development length decreases as Gr increases and is, for the conditions studied here, quite short: it varies from approximately 15 diameters for $Gr = 1.5 \times 10^5$ to 5 diameters for $Gr = 1.5 \times 10^6$. The order of magnitude of this length is qualitatively consistent with the corresponding result for forced convection (Shah and London, 1978) which indicates that the thermal development length is quite short for low Reynolds numbers.

The results of Figures 3a-d also show that, at any given axial position, the fluid temperature near the wall increases monotonically between the bottom ($\phi = -\pi/2$) and top ($\phi = \pi/2$) of the tube. This result is due to the y-component of the buoyancy force which creates a secondary flow in the xOy plane described in several earlier studies (Choudhury and Patankar, 1988; Orfi *et al.*, 1998; Ouzzane and Galanis, 1999). However, these studies, which use an axially parabolic formulation, cannot predict the preheating of the fluid in the adiabatic zone ($Z < 0$) which is clearly illustrated in Figures 3a-d. This effect has also been noted by Nesreddine *et al.* (1998) in a study of mixed convection in a vertical tube.

Figures 4-7 show the axial velocity profiles at four different cross-sections in the heating region ($Z/D = 0, 0.45, 1.7, 2.95$) for four different Grashof numbers. Parts a and b of each figure present the velocity profile in the y0z and xOz planes respectively. It should first be noted that the velocity profiles in the xOz plane are always symmetrical with respect to the tube axis. This observation is consistent with the overall symmetry of the problem with respect to the vertical plane which includes the tube axis. Secondly, it has been observed that both upstream ($Z/D = -6$) and far downstream ($Z/D > 50$) the velocity profiles in both planes under consideration are independent of the Grashof number and essentially identical to the Poiseuille parabolic distribution (these results are not presented here for lack of space). This is due to the fact that, at these axial positions, the fluid temperature is essentially uniform (see Figure 3) and the hydrodynamic field is developed.

On the other hand, the axial velocity profiles at the entry of the heating region ($Z/D = 0$) are not parabolic and are strongly influenced by the value of the Grashof number. This is particularly evident in part a of the figures. Thus for $Gr = 1.5 \times 10^5$ (Figure 4a) the velocity profile at $Z/D = 0$ has a maximum value of approximately

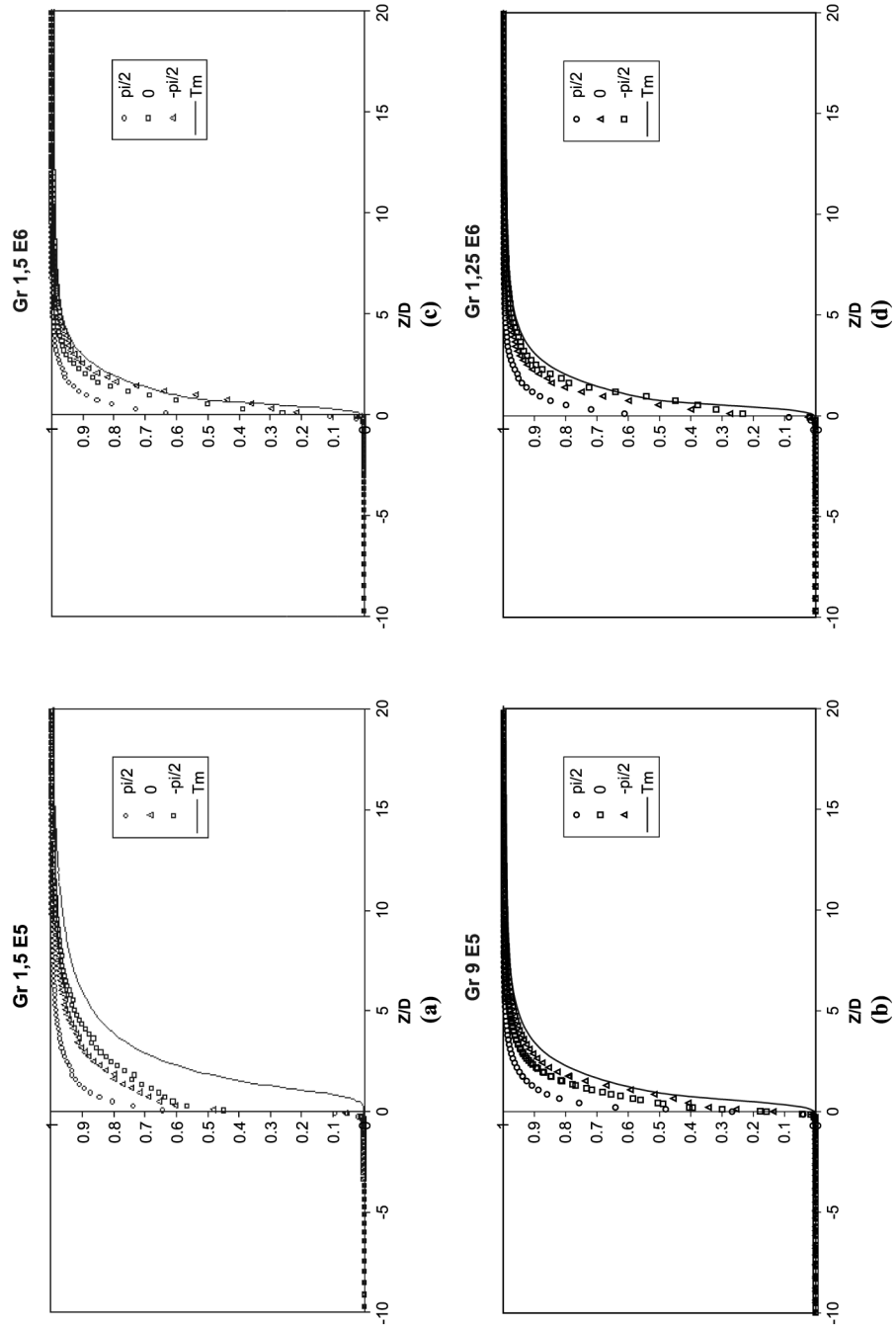

Figure 3.
Axial evolution of the non-dimensional fluid temperature

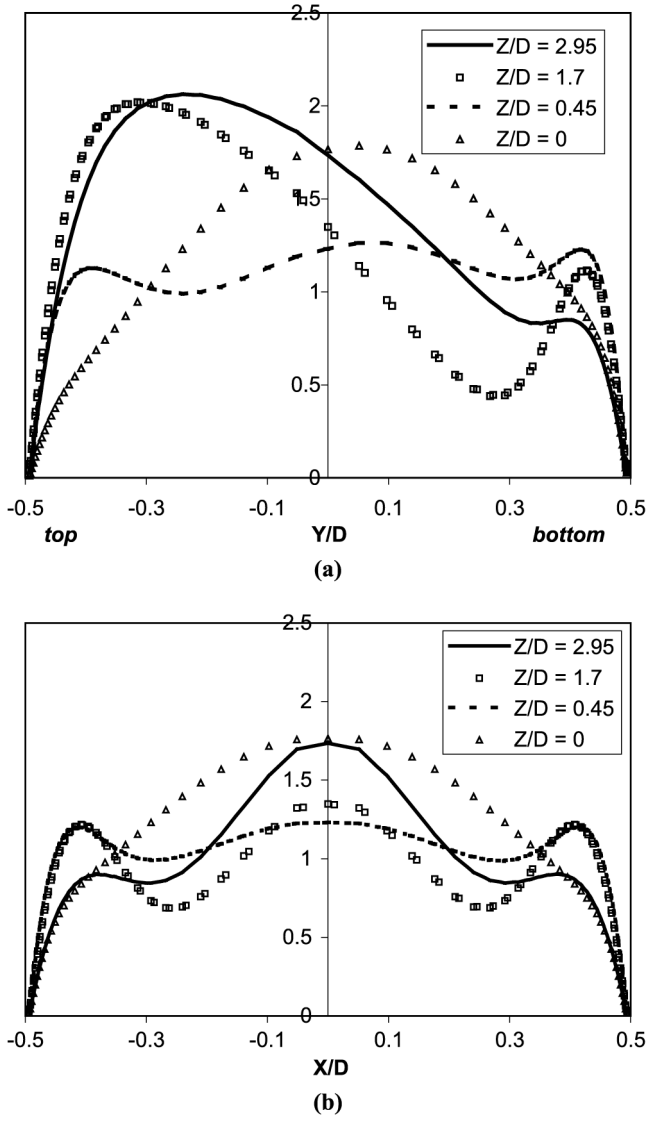

Figure 4.
Non-dimensional axial velocity profiles for $Gr = 1.5 \times 10^5$ in (a) yOz plane, (b) xOz plane

1.8 at $y/D \approx 0.05$ and decreases monotonically as $y/D \rightarrow \pm 0.5$. This is due to the fact that in this case the temperature difference $T_w - T_o$ is quite small. Therefore the corresponding natural convection effects are negligible and the velocity profile evolution between $Z/D = -10$ and $Z/D = 0$ is controlled by boundary layer growth. This explanation is reinforced by the observation that for this Grashof number the velocity profiles in Figures 4a-b are almost identical, suggesting that for these conditions ($Gr = 1.5 \times 10^5$, $Z/D = 0$) the velocity field is essentially axisymmetric. The situation at $Z/D = 0$ is completely different for the three other Grashof numbers.

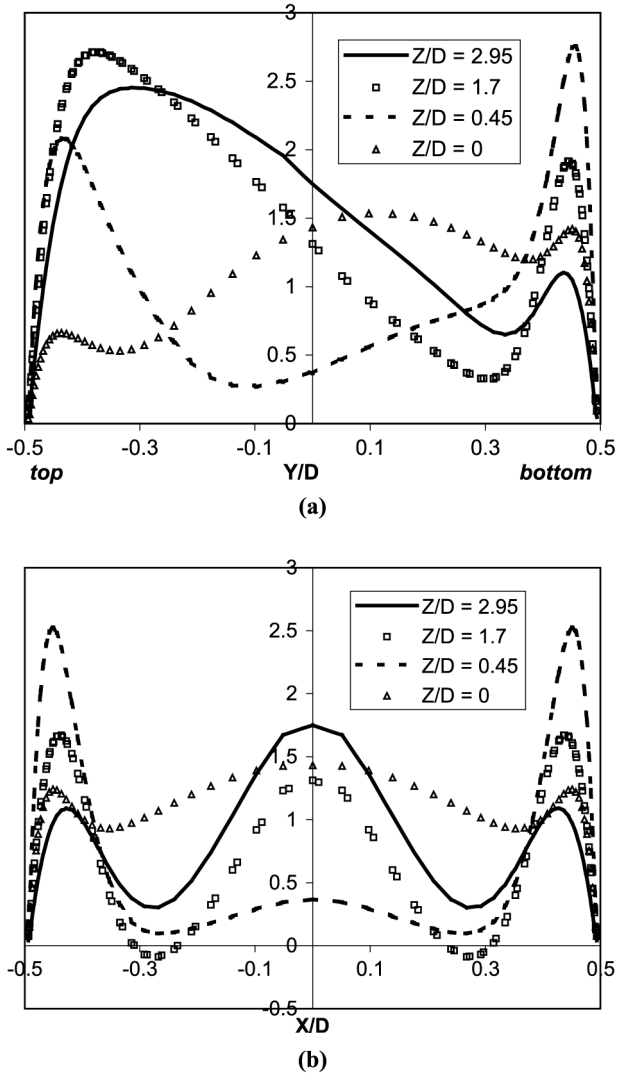

Figure 5.
Non-dimensional axial velocity profiles for $Gr = 9 \times 10^5$ in (a) yOz plane, (b) xOz plane

The velocity profiles in the vertical plane (part a of Figures 5-7) exhibit two local minima in the upper and lower halves of the tube. The maximum velocity occurs near the tube axis for $Gr = 9 \times 10^6$ (Figure 5a) and near the bottom of the wall for $Gr = 1.25 \times 10^6$ (Figure 6a) and $Gr = 1.5 \times 10^6$ (Figure 7a). These results indicate that, for those higher temperature differences $T_w - T_o$, the effects of natural convection created by the axial component of the buoyancy force play a significant role at the inlet of the heating region.

The preheating of the fluid in the adiabatic region and the dependence of the velocity profile at $Z = 0$ on the Grashof number illustrate the effects of axial diffusion

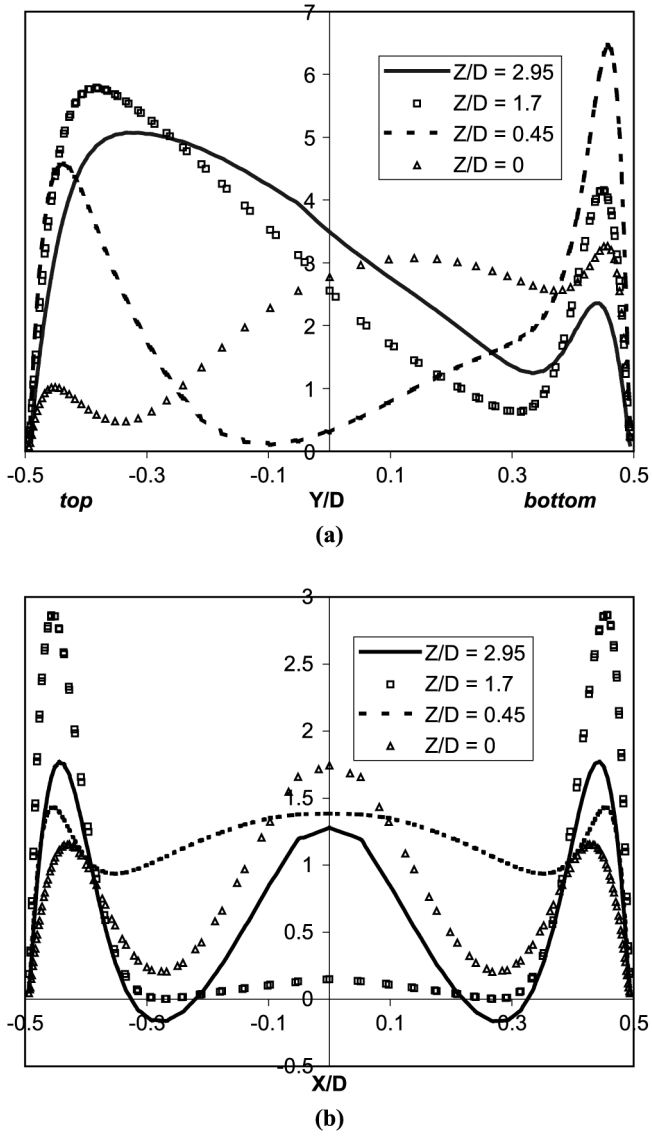

Figure 6.
Non-dimensional axial velocity profiles for $Gr = 1.25 \times 10^6$ in (a) yOz plane, (b) xOz plane

of heat and momentum. They clearly demonstrate the fact that, in situations such as those under consideration here, application of the inlet-boundary conditions at the beginning of the heated region ($Z = 0$) would mask some important phenomena as noted previously by Shah and London (1978).

Figures 5-7 corresponding to the three higher Grashof numbers under consideration also show that the axial velocity can be negative in some regions of the tube. For the

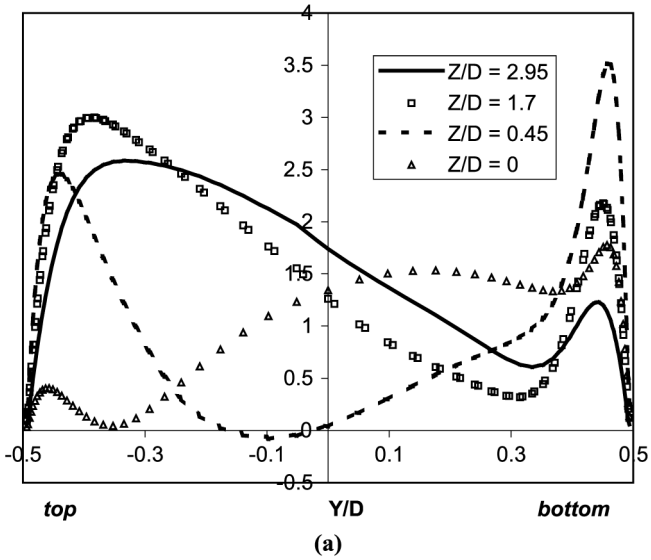

Figure 7.
Non-dimensional axial velocity profiles for $Gr = 1.5 \times 10^6$ in (a) yOz plane, (b) xOz plane

lowest Grashof number, $Gr = 1.5 \times 10^5$, negative velocities have not been observed. This manifestation of flow reversal occurs along the x axis at $Z/D = 1.7$ for $Gr = 9 \times 10^5$, and at $Z/D = 2.95$ for $Gr = 1.25 \times 10^6$. For $Gr = 1.5 \times 10^6$ it occurs along the y axis at $Z/D = 0.45$ as well as along the x axis at $Z/D = 0.45$ and $Z/D = 1.7$. Therefore the extent and shape of the region with negative velocities is considerably influenced by the value of the Grashof number. Figures 8-10 show side

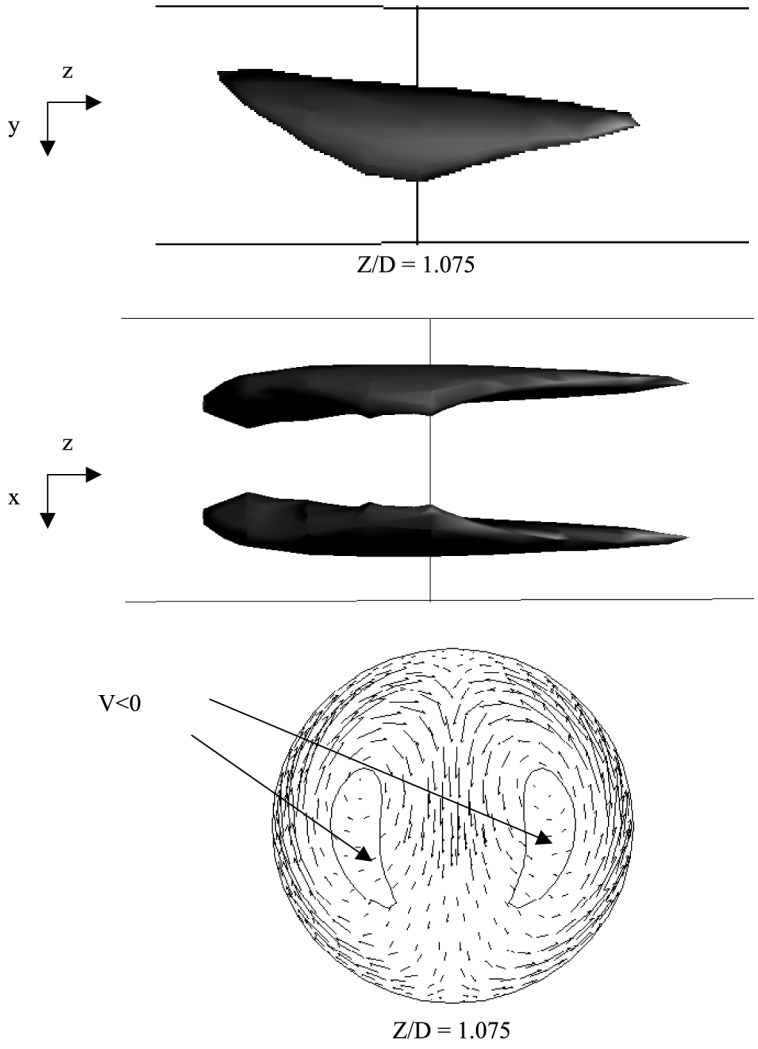

Figure 8.
Region of negative axial velocity for $Gr = 9 \times 10^5$

and top views of this region as well as its cross-sections at selected axial positions for three different Grashof numbers. The secondary flow generated by the y-component of the buoyancy force is also illustrated in these cross-sections. In all three cases this secondary flow consists of two symmetrical vortices. Hot fluid rises near the wall and descends near the vertical diameter. For $Gr = 9 \times 10^5$ (Figure 8) the region of negative axial velocities consists of two distinct, symmetrical, elongated ovoids with a kidney-shaped cross-section. For $Gr = 1.25 \times 10^6$ (Figure 9) the two ovoids are larger and join across the vertical plane of symmetry at half-length approximately. Finally, for $Gr = 1.5 \times 10^6$ (Figure 10) the two ovoids coalesce over the first half of their streamwise length. In all three cases, the upstream tip of the region with negative velocities is closer to the top of the tube than its downstream tip.

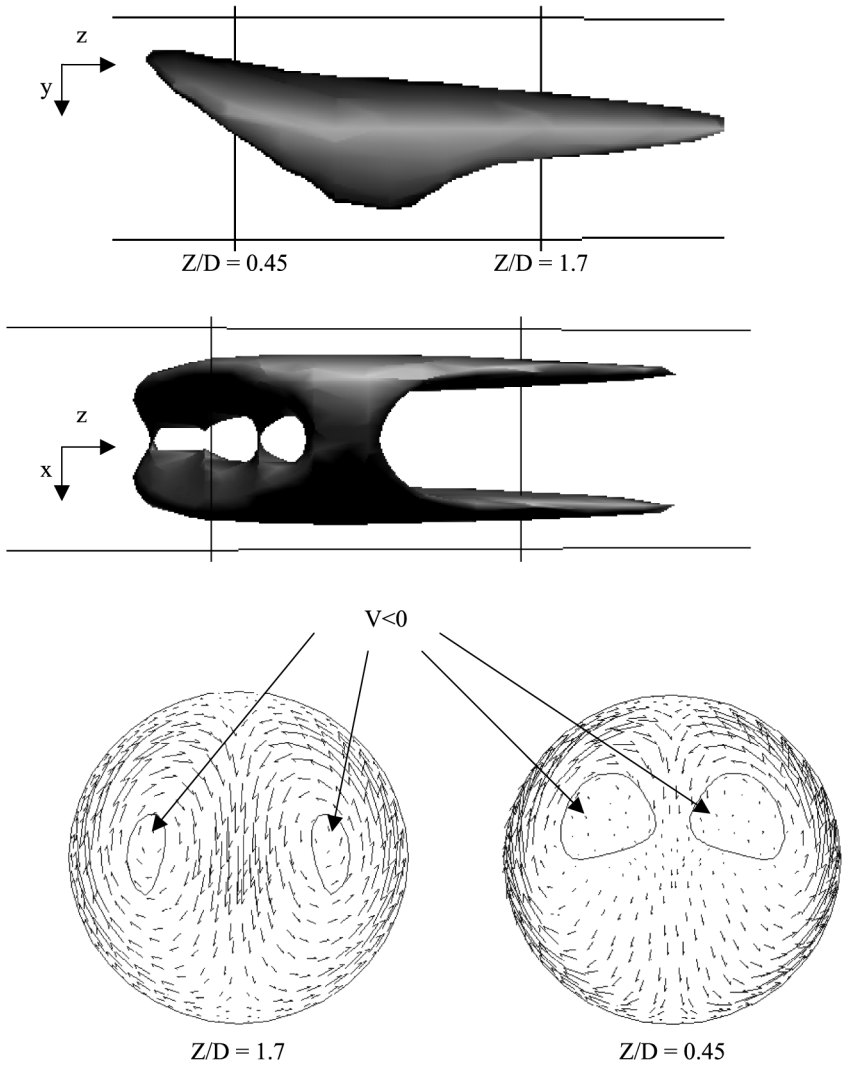

Figure 9.
Region of negative axial velocity for $Gr = 1.25 \times 10^6$

The hydrodynamic characteristics illustrated in Figures 4-10 influence the wall shear stress. Figure 11 shows the axial evolution of the circumferentially-averaged value of this parameter calculated from the expression:

$$\tau = \frac{1}{2\pi} \int_0^{2\pi} \frac{\partial V_Z}{\partial R} \, d\theta \tag{7}$$

Far upstream from the heated zone this parameter is independent of the Grashof number indicating that upstream diffusion does not have any influence for $Z/D < -1$. The numerically calculated value of τ in this upstream region is 8.02 which is very

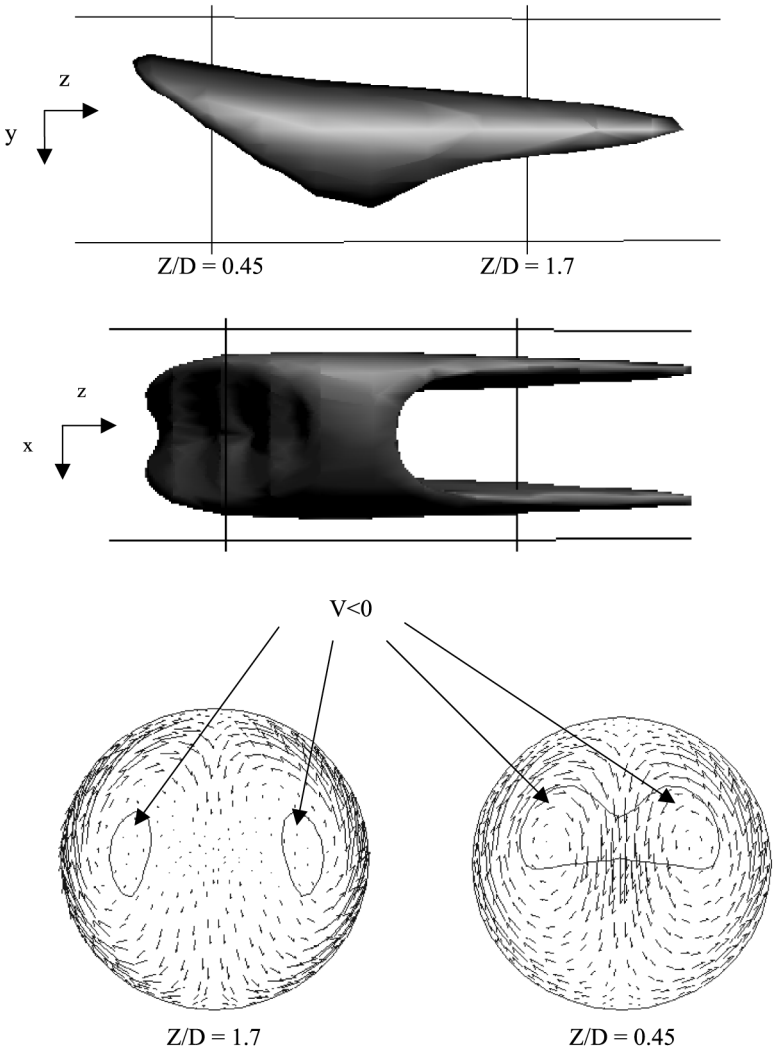

Figure 10.
Region of negative axial velocity for $Gr = 1.5 \times 10^6$

close to the corresponding value for fully developed forced convection ($\tau = 8$) confirming the earlier assertion that in this region the flow is isothermal and hydrodynamically developed. Just before the beginning of the heated region ($-1 < Z/D < 0$) however, the value of τ decreases slightly as a result of the upstream diffusion of heat and momentum described earlier. The minimum value in this region decreases as the Grashof number increases. Immediately after the beginning of the heated region ($Z/D > 0$) τ increases rapidly due to the accelerating effect of the axial component of the buoyancy force which generates high axial velocities in the vicinity of the solid-fluid interface (cf Figures 4-7). The shear stress reaches a maximum value which increases with the Grashof number. It then starts

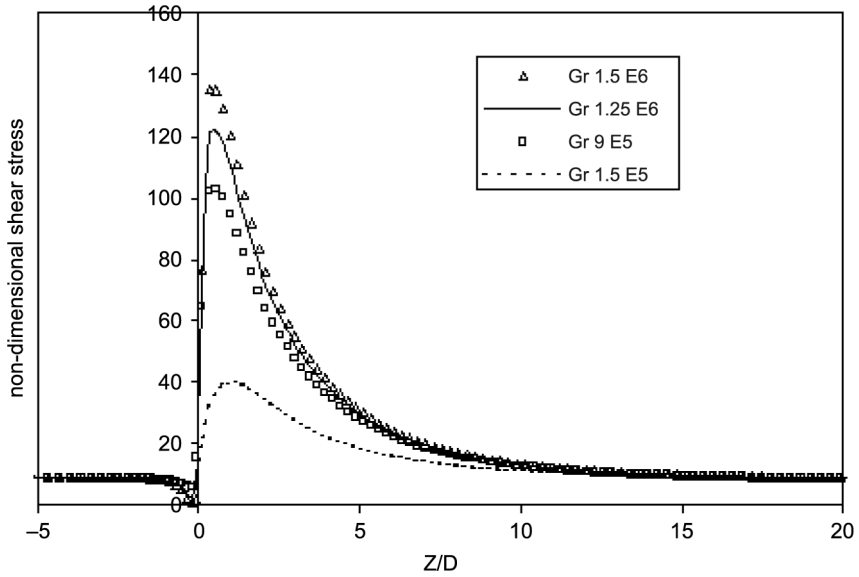

Figure 11.
Axial evolution of non-dimensional wall shear stress

decreasing as the temperature of the fluid tends towards a uniform value equal to the wall temperature and the velocity profile gradually approaches the fully-developed parabolic profile for isothermal flow. This tendency is substantiated by the fact that for $Z/D > 50$ the value of τ is independent of Gr and equal to 8.1, i.e. essentially equal to that for fully-developed forced convection. It should be noted, that for fully developed mixed convection in a uniformly heated tube the value of τ is higher and depends on the Grashof number (Ouzzane and Galanis, 1999)

Finally, Figure 12 presents the axial evolution of the circumferentially averaged Nusselt number calculated from the expression

$$\mathrm{Nu} = \frac{1}{2\pi} \frac{\int_0^{2\pi} \frac{\partial T}{\partial Z} \, \mathrm{d}\theta}{T_B - T_W} \tag{8}$$

Far upstream from the heating region its value is zero as expected. However, due to the afore-mentioned upstream diffusion, it becomes positive shortly before the beginning of the heating region. In the heating region it increases very rapidly and reaches a maximum value which increases as Gr increases. Beyond this point, the value of Nu decreases as the fluid temperature approaches the wall temperature and tends towards a value of 3.634 which is independent of Gr and very close to the corresponding value for forced convection. Throughout the developing region the value of Nu, at any given axial position, increases with Gr. It should be noted that the Nusselt number experiences a small sudden increase at the position where flow reversal occurs. This is attributed to an increase of bulk temperature caused by the upstream movement of warm fluid.

4. Conclusion

The numerical solution of the elliptical partial differential equations modelling upwards laminar mixed convection of air, heated in an inclined isothermal tube,

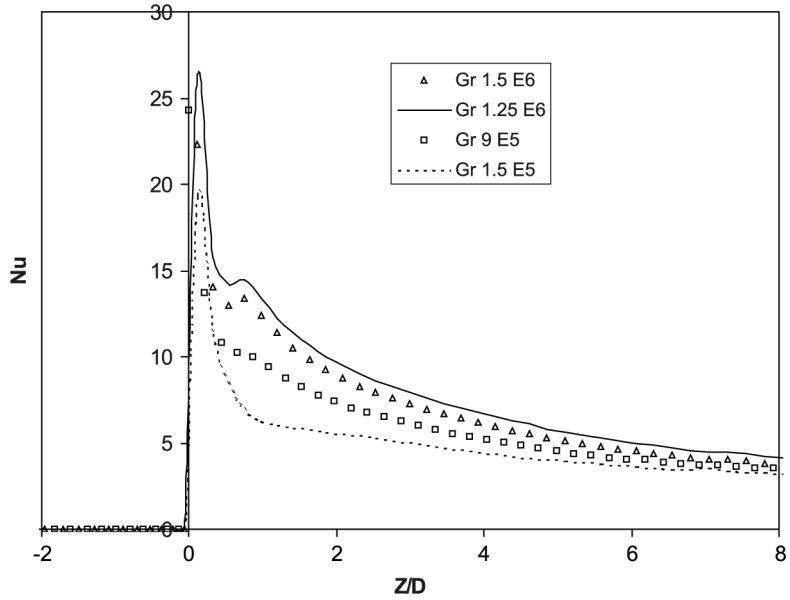

Figure 12.
Axial evolution of circumferentially averaged Nusselt number

has shown that for the conditions of this study ($Pr = 0.7$, $Re = 100$, $1.5 \times 10^5 \leq Gr \leq 1.5 \times 10^6$) axial diffusion plays an important role near the inlet of the heating region: namely, both the wall shear stress and the Nusselt number are affected upstream of the heating region. Furthermore, flow reversal has been observed for $Gr \geq 9 \times 10^5$. Neither of these effects had previously been reported for mixed convection in inclined tubes. The effect of the Grashof number on the wall shear stress and the Nusselt number was shown to be significant in the region of flow development.

References

Bernier, M. and Baliga, B.R. (1992), "Visualization of upward mixed convection flows in vertical pipes using a thin semi-transparent gold film heater and dye injection", *Int. J. Heat Fluid Flow*, Vol. 13, pp. 241-9.

Choudhury, D. and Patankar, S.V. (1988), "Combined forced and free laminar convection in the entrance region of an inclined isothermal tube", *ASME J. Heat Transfer*, Vol. 110, pp. 901-9.

Collins, M.W. (1980), "Finite difference analysis for developing laminar flow in circular tubes applied to forced and combinated convection", *Int. J. Num. Methods in Ingineering*, Vol. 15, pp. 381-404.

Fluent 6.1 User's Guide (n.d.), www.fluentusers.com

Nesreddine, H., Galanis, N. and Nguyen, C.T. (1995), "Recirculating flow in aiding/opposing mixed convection in vertical pipes", *Num. Methods Laminar Turbulent Flow*, Vol. 9, pp. 575-85.

Nesreddine, H., Galanis, N. and Nguyen, C.T. (1998), "Effects of axial diffusion on laminar heat transfer with low Péclet numbers in the entrance region of thin vertical tubes", *Num. Heat Transfer Pt. A*, Vol. 33, pp. 247-66.

Orfi, J., Galanis, N. and Nguyen, C.T. (1998), "Laminar mixed convection in the entrance region of inclined pipes with high uniform heat fluxes", *ASHRAE Transactions*, Vol. 104, pp. 417-28.

Ouzzane, M. and Galanis, N. (1999), "Effet de la conduction pariétale et de la répartition du flux thermique sur la convection mixte près de l'entrée d'une conduite inclinée", *Int. J. Therm. Sci.*, Vol. 38, pp. 622-33.

Pagliarini, G. (1989), "Steady laminar heat transfer in the entry region of circular tubes with axial diffusion of heat and momentum", *Int. J. Heat Mass Transfer*, Vol. 32, pp. 1037-52.

Patankar, S.V. and Spalding, D.B. (1972), "Calculation procedure for heat, mass and momentum transfer in three-dimensional parabolic flows", *Int. J. Heat Mass Transfer*, Vol. 15, pp. 1787-806.

Piva, S., Barozzi, G.S. and Collins, M.W. (2000), "Collins Combined free and forced convection in horizontal flows: a review, ch. 8", in Sunden, B. and Comini, G. (Eds), *Computational Analysis of Convection Heat Transfer*, WIT Press, Southampton.

Shah, R.K. and London, A.L. (1978), *Laminar flow forced convection in ducts, a source book for compact heat exchanger analytical data*, Academic Press, New York, NY.

Voicu, I.M. (2002), *Étude numérique du comportement aérothermique d'un fluide dans un tube isotherme en convection mixte, Rapport de projet de fin d'études*, Labo de thermique des bâtiments, IUT de Rennes.

Wang, M., Tsuji, T. and Nagano, Y. (1994), "Mixed convection with flow reversal in the thermal entrance region of horizontal and vertical pipes", *Int. J. Heat Mass Transfer*, Vol. 37, pp. 2305-19.

Zeldin, B. and Schmidt, F.W. (1972), "Developing flow with combined forced-free convection in an isothermal vertical tube", *ASME J. Heat Transfer*, Vol. 94, pp. 211-23.

Zghal, M., Galanis, N. and Nguyen, C.T. (2001), "Developing mixed convection with aiding buoyancy in vertical tubes: a numerical investigation of different flow regimes", *Int. J. Therm. Sci.*, Vol. 40, pp. 816-24.